

# Non-Hermitian topological superfluid in a three dimensional optical lattice

Pingcheng Zhu, Lihong Zhou,\* and Jianxin Zhong†

*Institute for Quantum Science and Technology, Shanghai University, Shanghai 200444, China*

(Dated: January 6, 2026)

The experimental advances in realizing artificial spin-orbit coupling (SOC) and non-Hermitian potentials in ultracold atomic system open a new avenue for exploring their significant roles in quantum many-body physics. Here, we investigate a non-Hermitian, two-component Fermi system in a cubic lattice with Rashba SOC and complex-valued interaction arising from two-body loss. We adopt the non-Hermitian mean field theory and map out the phase diagram at zero temperature. The interplay of dissipation and on-site interaction drives a dissipation-induced phase transition from superfluid (SF) to normal phase (N). Notably, for weak interaction strengths, this leads to a reentrance of the superfluid state. The presence of SOC significantly expands the parameter regime for both the normal phase and the metastable superfluid phase(MSF). Whereas, the Zeeman field can drive the system from a conventional superfluid into a topological superfluid phase(TSF), characterized by a nontrivial topological invariant. These results enrich our knowledge of pairing superfluidity in Fermi systems.

## I. INTRODUCTION

Mostly, the real physical systems are inevitably open quantum systems due to their inescapable coupling to the environment. In recent decades, with the deepening of research on non-Hermitian quantum systems, the exploration of non-Hermitian physics has emerged as a vibrant frontier in modern physics, with profound implications across condensed matter, photonics, and atomic systems. It has been found that such systems can exhibit a wealth of exotic phenomena, such as exceptional points [1–4], the non-Hermitian skin effect [5–11]. Ultracold atomic gases, with their high controllability, provide an ideal platform for studying non-Hermitian physics, where the interaction is tunable through Feshbach resonances [12], the laser-induced synthetic SOC [13–16] and the non-Hermiticity can be realized in experiment via laser or electronic beam induced one-body [10, 17–22] or two-body dissipation [23–26]. Two-body dissipation refers to a class of decay processes in which two particles are simultaneously lost from the system due to their mutual interaction. Formally, this type of dissipation is described by introducing a complex-valued interaction into the system’s Hamiltonian, and the strength of two-body dissipation can be tuned by adjusting the depth of the optical lattice [23–26] in experiment. Theoretically, it has been shown that in the few-body regime, the non-Hermiticity arising from two-body dissipation acts to suppress the formation of both two- and three-body bound states [27, 28], which is contrast sharply with other types of non-Hermiticity—such as an imaginary magnetic field or non-Hermitian SOC acting at the single-particle level—which facilitate the formation of bound states [29–31]. While for the case of many-body physics, the theoretical studies demonstrate that two-body dissipation

can induce intriguing forms of fermion superfluidity, including dissipation-induced the phenomenon of superfluid reentrance [32–34] and phase transitions [24, 26, 35–37], and novel physics [38, 39].

Extensive research has explored the many-body effects of two-body dissipation in both lattice and continuum systems. However, most of these studies focus on the interplay between non-Hermiticity and interactions, the role of SOC and Zeeman fields in such dissipative settings has rarely been addressed. In particular, SOC Fermi gases serve as a unique platform for studying topological superfluidity [40–43] and exotic pairing mechanisms [44]. Therefore, investigating nontrivial phenomena arising from the interplay between SOC and non-Hermiticity is highly desirable.

In this work, we consider a two-component Fermi gas in a cubic lattice with Rahsba SOC, Zeeman field and a complex valued s-wave interaction. Within the framework of a mean-field approach, we determine the ground state of the system at zero temperature and construct the corresponding phase diagram. We demonstrate that such a system exhibits the interesting many-body physics affected by two-body dissipation and SOC. A fundamental feature of this system is the reentrant behavior of the superfluid state under weak interactions. While in lattice systems, either SOC or a Zeeman field alone tends to suppress pairing by increasing the single-particle band gap, their combined effect can be strikingly different. This interplay robustly drives and stabilizes the topological superfluid state. Our results enrich the physical picture and pave the way for understanding the open quantum many-body systems.

This work is organized as follows. In Sec. II we introduce the non-Hermitian effective Hamiltonian of the two-component system and derive the thermodynamic potential at zero temperature limit. We then obtain the gap equation and study the zero-temperature phase diagram in Sec. III. We first examine the phase diagram in the interaction-dissipation plane in the absence of a Zeeman field. Subsequently, we introduce a Zeeman field and

\* lihongzh@shu.edu.cn

† jxzhong@shu.edu.cn

investigate the phase diagram in the dissipation-Zeeman field plane at a fixed interaction strength. Finally, We summarize our work in Sec. IV.

## II. MODEL HAMILTONIAN

We consider a two-component Fermi system with Rashba SOC and a Zeeman field in a three-dimensional(3D) cubic lattice with lattice constant  $a$  [45–47], where particles with opposite pseudospins experience a complex valued s-wave interaction. The Hamiltonian can be written as

$$H = \int d\mathbf{r} \psi^\dagger(\mathbf{r}) \left[ H_0(\mathbf{r}) - h\sigma_z + \lambda(\hat{k}_y\sigma_x - \hat{k}_x\sigma_y) \right] \psi(\mathbf{r}) - g \int d\mathbf{r} \psi_\uparrow^\dagger(\mathbf{r}) \psi_\downarrow^\dagger(\mathbf{r}) \psi_\downarrow(\mathbf{r}) \psi_\uparrow(\mathbf{r}), \quad (1)$$

with

$$H_0(\mathbf{r}) = -\frac{\hbar^2 \nabla^2}{2m} - \mu + V_L(\mathbf{r}) \quad (2)$$

here the chemical potential  $\mu$  is determined by the total number of atoms  $N$  of the system. The optical-dipole potential  $V_L(\mathbf{r}) = V_0[\cos^2(k_L x) + \cos^2(k_L y) + \cos^2(k_L z)]$  forms the cubic lattice,  $V_0$  is the lattice depth and  $k_L$  is the recoil momentum giving the lattice spacing  $a = \frac{\pi}{k_L}$ . The operator  $\psi(\mathbf{r}) = [\psi_\uparrow(\mathbf{r}), \psi_\downarrow(\mathbf{r})]^T$  denotes collectively the annihilation operator for spin-up and spin-down atoms. Here,  $h$  is the strength of the Zeeman field and  $\lambda$  is the Rashba SOC constant,  $\hat{k}_i = -i\partial/\partial i$ , ( $i = x, y, z$ ) is the momentum operator,  $\sigma_i$  is the  $2 \times 2$  Pauli matrix, and  $g$  represents the 3D interaction constant.

To capture the low-energy physics in deep lattices, the conventional approach is to expand the field operator in terms of the Wannier functions of the lowest band  $\psi_\sigma(\mathbf{r}) = \sum_j w_{n=0}(\mathbf{r} - \mathbf{r}_j) c_{j\sigma}$  ( $n$  is the band index,  $\sigma$  is spin and  $j = (j_x, j_y, j_z)$  is 3D lattice site), the mixing between lower and upper bands is neglected. The tight-binding model of the Hamiltonian can be derived

straightly

$$H = -t \sum_{\langle ij \rangle \sigma} c_{i\sigma}^\dagger c_{j\sigma} - \sum_{i\sigma} (\mu + h\sigma_z) c_{i\sigma}^\dagger c_{i\sigma} - U \sum_{\vec{i}} c_{i\uparrow}^\dagger c_{i\downarrow}^\dagger c_{i\downarrow} c_{i\uparrow} + \alpha \sum_{j_x} [(c_{j_x\uparrow}^\dagger c_{j_x+1\downarrow} - c_{j_x+1\uparrow}^\dagger c_{j_x\downarrow}) + H.C.] - i\alpha \sum_{j_y} [(c_{j_y\uparrow}^\dagger c_{j_y+1\downarrow} - c_{j_y+1\uparrow}^\dagger c_{j_y\downarrow}) + H.C.] \quad (3)$$

where  $c_{i\sigma}$  ( $c_{i\sigma}^\dagger$ ) is the annihilation (creation) operator of the fermion at site  $\vec{i}$ . The on-site interaction  $U = U_1 + i\gamma/2$  is complex-valued, incorporating the interaction strength  $U_1$  and the two-body loss rate  $\gamma$ , where  $U_1, \gamma > 0$ . The nearest-neighbor hopping term  $t = -\int d^3 \mathbf{r} w_0^*(\mathbf{r} - \mathbf{r}_i) [\frac{\hbar^2 \nabla^2}{2m} + V_L(\mathbf{r})] w_0(\mathbf{r} - \mathbf{r}_{i+1})$  and the spin-flip hopping terms due to the Rashba SOC satisfy  $\alpha = \lambda \int d^3 \mathbf{r} w_0^*(\mathbf{r} - \mathbf{r}_i) \frac{\partial}{\partial x} w_0(\mathbf{r} - \mathbf{r}_{i+1})$ .

Next, we can express the Hamiltonian of the system in quasi momentum space

$$H = \sum_{\mathbf{k}\sigma} \xi_{\mathbf{k}\sigma} c_{\mathbf{k}\sigma}^\dagger c_{\mathbf{k}\sigma} + \sum_{\mathbf{k}\sigma\sigma'} 2\alpha(\sigma_x \sin k_y - \sigma_y \sin k_x) c_{\mathbf{k}\sigma}^\dagger c_{\mathbf{k}\sigma'} - \frac{U}{N} \sum_{\mathbf{kk}'\mathbf{q}} c_{\mathbf{k}+\mathbf{q}/2\uparrow}^\dagger c_{-\mathbf{k}+\mathbf{q}/2\downarrow}^\dagger c_{-\mathbf{k}'+\mathbf{q}/2\downarrow} c_{\mathbf{k}'+\mathbf{q}/2\uparrow}, \quad (4)$$

where  $\xi_{\mathbf{k}\uparrow} = \xi_{\mathbf{k}} \mp h$  and  $\xi_{\mathbf{k}} = -2t(\cos k_x + \cos k_y + \cos k_z) - \mu$  is the single-particle dispersion relation in the optical lattice.

In the following discussion, we take the non-Hermitian mean-field approximation to the interaction term and consider the most representative case of zero center-of-mass momentum  $q = 0$ . The non-Hermitian mean field order parameters are defined as

$$\Delta = -\frac{U}{N} \sum_{\mathbf{k}} {}_L \langle c_{-\mathbf{k}\downarrow} c_{\mathbf{k}\uparrow} \rangle_R, \quad \tilde{\Delta} = -\frac{U}{N} \sum_{\mathbf{k}} {}_L \langle c_{\mathbf{k}\uparrow}^\dagger c_{-\mathbf{k}\downarrow}^\dagger \rangle_R. \quad (5)$$

where  $|E_n\rangle_{R(L)}$  refers to the right (left) eigenstates of Hamiltonian  $H(H^\dagger)$  with energy  $E_n(E_n^*)$ , and  $|E_n\rangle_R \neq |E_n\rangle_L$ , indicating  $\Delta$  and  $\tilde{\Delta}$  are not complex conjugate to each other.

Then the mean-field Hamiltonian in the Nambu basis  $\Psi_{\mathbf{k}} = (c_{\mathbf{k}\uparrow}, c_{\mathbf{k}\downarrow}, c_{-\mathbf{k}\uparrow}^\dagger, c_{-\mathbf{k}\downarrow}^\dagger)^T$  can be expressed as

$$H_{\text{MF}} = \frac{1}{2} \sum_{\mathbf{k}} \Psi_{\mathbf{k}}^\dagger M_{\mathbf{k}} \Psi_{\mathbf{k}} + \frac{1}{2} \sum_{\mathbf{k}} (\xi_{\mathbf{k}\uparrow} + \xi_{\mathbf{k}\downarrow}) + \frac{N}{U} \Delta \tilde{\Delta} \quad (6)$$

where the corresponding Bogoliubov Hamiltonian

$$M_{\mathbf{k}} = \begin{pmatrix} \xi_{\mathbf{k}\uparrow} & 2\alpha(\sin k_y + i\sin k_x) & 0 & \Delta \\ 2\alpha(\sin k_y - i\sin k_x) & \xi_{\mathbf{k}\downarrow} & -\Delta & 0 \\ 0 & -\tilde{\Delta} & -\xi_{\mathbf{k}\uparrow} & -2\alpha(\sin k_y - i\sin k_x) \\ \tilde{\Delta} & 0 & -2\alpha(\sin k_y + i\sin k_x) & -\xi_{\mathbf{k}\downarrow} \end{pmatrix} \quad (7)$$

Once the superfluid is formed, there is a spontaneous U(1) symmetry breaking and the order parameter obtain a phase. By choosing a specific gauge for which the phase difference of the two order parameters vanishes, we have  $\Delta = \tilde{\Delta} = \Delta_0$ . The mean-field Hamiltonian can be diagonalized as

$$H_{\text{MF}} = \frac{1}{2} \sum_{\mathbf{k}, \nu=\pm} (E_{\mathbf{k}\nu} \bar{\alpha}_{\mathbf{k}\nu} \alpha_{\mathbf{k}\nu} + E_{\mathbf{k}\nu} \bar{\beta}_{\mathbf{k}\nu} \beta_{\mathbf{k}\nu}) + \frac{N}{U} \Delta_0^2 + \sum_{\mathbf{k}} [\xi_{\mathbf{k}} - \frac{1}{2}(E_{\mathbf{k}+} + E_{\mathbf{k}-})] \quad (8)$$

where the quasiparticle energy spectrum is given by

$$E_{\mathbf{k}\pm} = \sqrt{\xi_{\mathbf{k}}^2 + \Delta_0^2 + h^2 + 4\alpha^2(\sin^2 k_x + \sin^2 k_y)} \pm 2E_0$$

with  $E_0 = \sqrt{(h^2 + 4\alpha^2(\sin^2 k_x + \sin^2 k_y)) \xi_{\mathbf{k}}^2 + h^2 \Delta_0^2}$ .  $\bar{\alpha}_{\mathbf{k}\nu}(\bar{\beta}_{\mathbf{k}\nu})$  and  $\alpha_{\mathbf{k}\nu}(\beta_{\mathbf{k}\nu})$  is the quasiparticle (hole) operator for different helicities, which satisfies the anti-commutation relation  $\{\bar{\alpha}_{\mathbf{k}\nu}, \alpha_{\mathbf{k}'\nu'}\} = \delta_{\mathbf{k}\mathbf{k}'} \delta_{\nu\nu'}$ .

To elucidate the many-body physics of the quantum open system, we consider the grand partition function

$$\mathcal{Z}_{\text{MF}} = \prod_{\mathbf{k}, \nu=\pm} (1 + e^{-\beta E_{\mathbf{k}\nu}})(1 + e^{\beta E_{\mathbf{k}\nu}}) \times e^{-\beta [\xi_{\mathbf{k}} - (E_{\mathbf{k}+} + E_{\mathbf{k}-})/2] e^{-\beta N \Delta_0^2/U}}, \quad (9)$$

where  $\beta = 1/k_B T$  denotes the inverse temperature. The thermodynamic potential can be obtained from  $\Omega_{\text{MF}} = -\frac{1}{\beta} \ln \mathcal{Z}_{\text{MF}}$

$$\Omega_{\text{MF}} = -\frac{1}{\beta} \sum_{\mathbf{k}, \nu=\pm} \ln(1 + e^{-\beta E_{\mathbf{k}\nu}})(1 + e^{\beta E_{\mathbf{k}\nu}}) + \sum_{\mathbf{k}} \left[ \xi_{\mathbf{k}} - \frac{1}{2}(E_{\mathbf{k}+} + E_{\mathbf{k}-}) \right] + \frac{N}{U} \Delta_0^2, \quad (10)$$

In this work, we consider the limit  $\beta \rightarrow \infty$  to elucidate the ground-state physics. At zero temperature, the thermodynamic potential reduces to

$$\Omega_{\text{MF}} = \sum_{\mathbf{k}} [E_{\mathbf{k}+} \Theta(-\text{Re}(E_{\mathbf{k}+})) + E_{\mathbf{k}-} \Theta(-\text{Re}(E_{\mathbf{k}-}))] + \sum_{\mathbf{k}} \left[ \xi_{\mathbf{k}} - \frac{1}{2}(E_{\mathbf{k}+} + E_{\mathbf{k}-}) \right] + \frac{N}{U} \Delta_0^2. \quad (11)$$

### III. PHASE DIAGRAM

To construct the zero-temperature phase diagram, we derive the gap equation from the stationary condition of

the thermodynamic potential  $\partial \Omega_{\text{MF}} / \partial \Delta_0 = 0$ ,

$$\frac{N}{U} = \sum_{\mathbf{k}} \left( \frac{1 + h^2/E_0}{4E_{\mathbf{k}+}} + \frac{1 - h^2/E_0}{4E_{\mathbf{k}-}} \right). \quad (12)$$

The order parameters are obtained by solving the gap equation for different choices of interaction strength  $U_1$ , dissipation  $\gamma$ , SOC strength  $\alpha$  and Zeeman field  $h$ . To distinguish different phases, we resort to a method based on the energy difference between the superfluid state and the normal state as  $\Delta E = \Omega_{\text{MF}}(\Delta_0) - \Omega_{\text{MF}}(0)$  [32, 34]. In the following numerical calculations, we adopt the hopping integral  $t$  and the lattice constant  $a$  as units of energy and length, respectively.

We first investigate the effect of Rashba SOC. In Fig. 1, we present the mean-field zero-temperature phase diagram in the interaction strength–dissipation plane ( $U_1, \gamma$ ) for different SOC strength, and elucidate the intricate interplay between the interaction strength, dissipation, and SOC. The yellow region corresponds to the stable normal phase (N), characterized by  $\text{Re}(\Delta_0) = 0$ . The blue region represents the stable superfluid phase (SF), distinguished by  $\text{Re}(\Delta_0) \neq 0$  and  $\Delta E < 0$ , which is an effective ground state of the non-Hermitian Hamiltonian. The light blue region denotes the metastable superfluid phase (MSF), identified by  $\text{Re}(\Delta_0) \neq 0$  and  $\Delta E > 0$ . An interesting phase occurs in the weakly interacting regime. As dissipation increases, the system undergoes a sequence of phase transitions: from the superfluid phase to the metastable superfluid phase, and finally to the normal phase. Upon further increasing the dissipation strength, the system re-enters the metastable superfluid phase. This reentrant behavior is a direct consequence of the quantum Zeno effect [23, 24]: strong two-body dissipation suppresses intersite particle hopping, favors on-site pair formation, and thereby enhances the superfluid order parameter. The physical mechanism is the same as that discussed in Ref. [32, 34]. Another characteristic feature across all three figures illustrated in panels Fig. 1(a) to (c) is that, as the SOC strength increases — the areas of both the normal and metastable superfluid phases expand, while the region of the stable superfluid phase shrinks. This suppression of superfluidity by SOC can be understood from the single-particle energy spectrum.

To gain deeper insights into the phase transition in the weak-interaction regime, in Figs. 2 (a) and (b) we present the real part of the order parameter  $\Delta_0$  and the condensate energy  $\Delta E$  as functions of dissipation  $\gamma$  with different SOC strength. As shown in Fig. 2 (a), the real part of the order parameter vanishes as dissipation increases, indicating that the superfluid state is destroyed

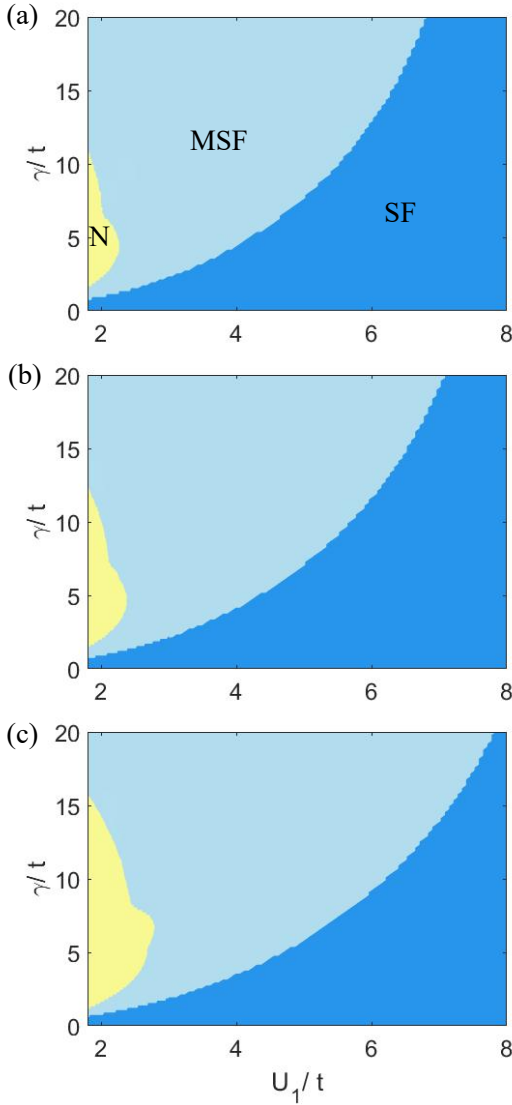


FIG. 1. Zero-temperature phase diagram in the parameter space of the interaction strength  $U_1$  and the dissipation  $\gamma$  with the spin-orbit coupling strength: (a)  $\alpha/t = 0$ , (b)  $\alpha/t = 0.4$ , and (c)  $\alpha/t = 0.8$ . The blue, light blue, and yellow regions denote stable superfluid, metastable superfluid, and normal states, respectively. In all figures we take  $\mu/t = 0$ ,  $h/t = 0$ . Due to numerical constraints, the region with small  $U_1$  is not shown.

and the system enters the normal state. However, with further increased dissipation, the superfluid state recovers and the order parameter rises. The corresponding condensate energy starts from a negative value, increases with dissipation, and jumps discontinuously to zero; in the strong-dissipation regime, it turns positive again, indicating the existence of a metastable superfluid state, as shown in Fig. 2(b). In both Figs. 2(a) and (b), SOC expands the parameter regimes in which  $\Delta_0$  and  $\Delta E$  vanishes, thereby enlarging the area of the normal state and

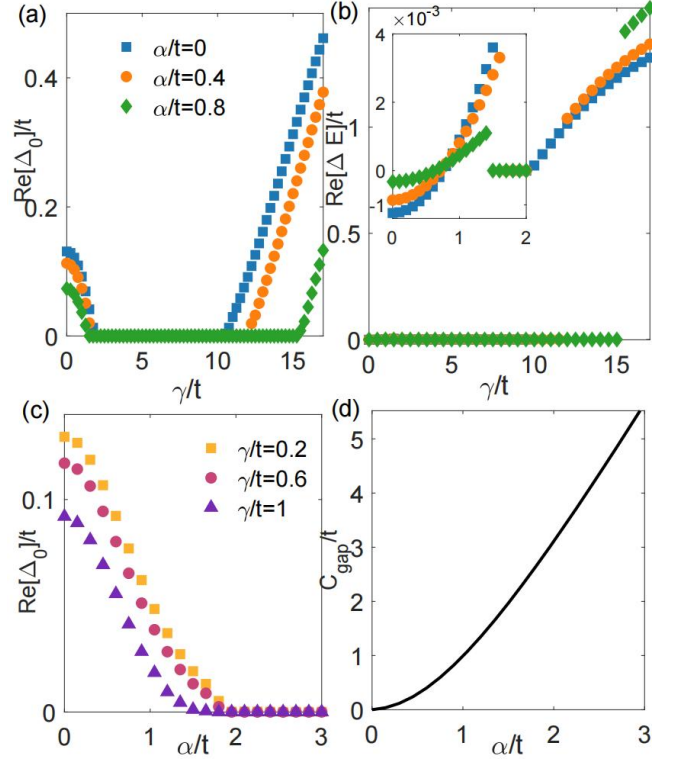


FIG. 2. The real parts of (a) order parameter  $\Delta_0/t$  and (b) condensate energy  $\Delta E/t$  as functions of the dissipation  $\gamma$  for SOC strength  $\alpha/t = (0, 0.4, 0.8)$ . The inset in (b) provides a magnified view at low dissipation strengths. (c) The real parts of order parameter  $\Delta_0/t$  as a function of SOC strength  $\alpha$  with  $\gamma/t = (0.2, 0.6, 1)$ . (d) The energy gap of the single-particle spectrum as a function of the spin-orbit coupling strength  $\alpha$ . In all figures we take  $\mu/t = 0$ ,  $U_1/t = 1.8$  and  $h/t = 0$ .

suppressing the superfluid phase. This inhibitory role of SOC is further illustrated in Fig. 2(c) and (d), where the order parameter decreases and the energy gap of a single-particle spectrum increases with increasing SOC strength. In the presence of SOC, the single-particle spectrum splits into two helicity branches. The monotonic increase of the energy gap in these two branches implies a reduced probability of inter-branch pairing.

The Zeeman field is also a commonly used tuning parameter that breaks spin degeneracy, modifies the energy-level structure, and thereby influences the pairing mechanism, phase diagram, and topological properties of the system. In experiments, the topological band structure has been observed by combinations of optical lattice, Zeeman field and SOC [48, 49]. To elucidate the intricate interplay of dissipation, Zeeman field and SOC, we present the zero-temperature phase diagram in the plane of Zeeman field strength and dissipation ( $h, \gamma$ ) for two different SOC strength in Fig. 3. Specially, we identify a new phase: a topological superfluid state characterized by a non-zero Chern number ( $C$ ) in the  $k_z$ -plane. This integer topological invariant serves as an effective predictor of the topological transition. In Fig. 3, regions with

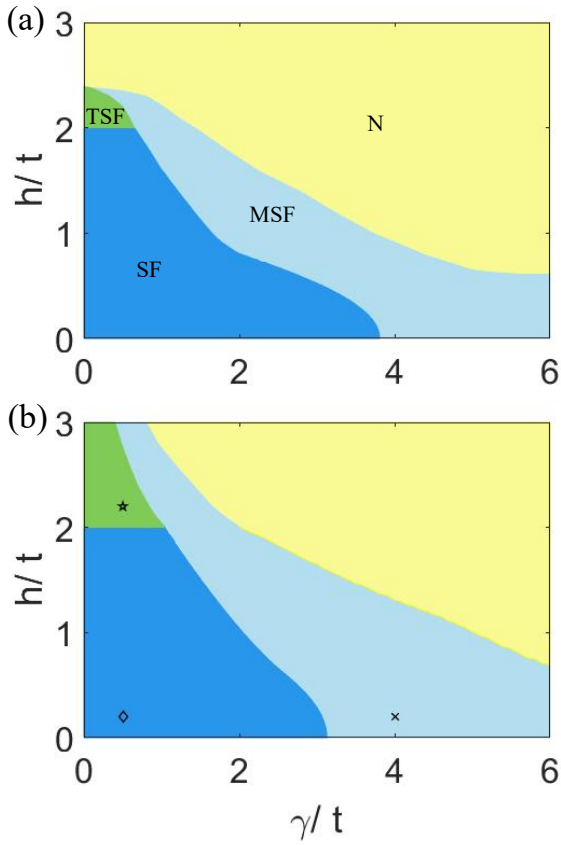


FIG. 3. Zero-temperature phase diagram in the plane of the dissipation  $\gamma$  and Zeeman field  $h$  with the SOC strength: (a)  $\alpha/t = 0.6$ , (b)  $\alpha/t = 1$ . The green region shows the topological superfluid phase. In all figures we take  $U_1/t = 4$  and  $\mu/t = 0$ .

$C \neq 0$  (indicated in green region) mark the topological superfluid phase. The interplay of SOC and Zeeman field splits the single-particle energy spectrum into distinct helical branches, enabling effective p-wave pairing and facilitating the emergence of the topological superfluid phase. For weak SOC as shown in Fig. 3(a), the topological superfluid phase is confined to a narrow window between the normal and trivial superfluid phases. Upon increasing SOC, this topological region broadens markedly, accompanied by a concomitant shrinkage of the trivial superfluid phase. This behavior can be attributed to the Rashba SOC operating through different mechanisms under varying Zeeman field strengths. For a weak Zeeman field, the Fermi surface mismatch between spin species is minimal. Here, the dominant pairing channel remains the zero-momentum, spin-singlet-like BCS state. For a large Zeeman field, the Fermi surfaces are severely shifted, causing a pronounced Fermi surface mismatch. This strongly suppresses and can completely destroy the conventional BCS pairing, the interplay of SOC and Zeeman field pushing the system toward a novel phase. In this regime, the SOC plays a constructive and

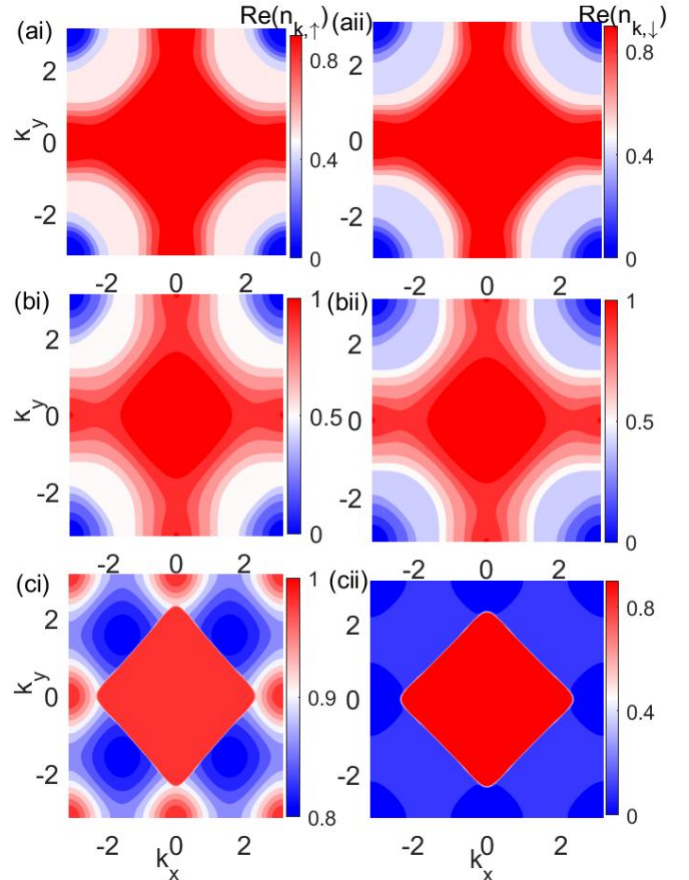


FIG. 4. The momentum space density distribution in  $k_z = 0$  plane for three phase marked in Fig. 3(b). The order parameters are (a)  $\Delta_0/t = 0.855 + 0.127i$  (superfluid phase), (b)  $\Delta_0/t = 0.755 + 1.087i$  (metastable superfluid phase), (c)  $\Delta_0/t = 0.016 + 0.008i$  (topological superfluid phase), other parameters are the same as Fig. 3(b).

essential role. Increasing the SOC strength in this regime enhances the efficiency of this alternative pairing channel. It increases the phase space available for forming these resilient pairs, which are immune to the large Zeeman field. This can be viewed as SOC engineering a path to superfluidity—such as a helical superfluid or a topological phase—that explicitly relies on strong spin-orbit interaction to exist. The crossover between these two regimes marks a transition in the dominant pairing mechanism. At a critical Zeeman field, the system moves from a topologically trivial BCS-like superfluid toward a non-trivial superfluid phase. In the latter, the order parameter may even originate from inter-band pairing and exhibit topological properties. Spin-orbit coupling serves as the cornerstone for designing topological phases, while the Zeeman field acts as a switch for controlling them. Their interplay effect is key to exploring novel topological quantum states and realizing future low-energy electronic devices.

It is well known that topological phases are typically characterized by topologically protected surface or edge

states. For lattice models, the phase boundary can be determined by the closure of the excitation gap [50]. According to quasiparticle energy spectrum, the excitation energy gap closes at  $h = \text{Re}\sqrt{\xi_k^2 + \Delta_0^2}$  with  $k_x = (0, \pm\pi)$ ,  $k_y = (0, \pm\pi)$ , corresponding to the following three conditions

$$h_c = \text{Re} \begin{cases} \sqrt{(-4t + 2t \cos(k_z) + \mu)^2 + \Delta_0^2} \\ \sqrt{(2t \cos(k_z) + \mu)^2 + \Delta_0^2} \\ \sqrt{(4t + 2t \cos(k_z) + \mu)^2 + \Delta_0^2} \end{cases} \quad (13)$$

Based on the Eq.(13), we can get the critical Zeeman fields at a fixed  $k_z$  value.

Complementary insight into the different phases can be gained from the zero-temperature momentum-space density distribution for each spin species, which is obtained from the derivative of the thermodynamic potential with respect to the corresponding chemical potential,  $n_\uparrow = -\partial\Omega_{\text{MF}}/\partial\mu_\uparrow$  and  $n_\downarrow = -\partial\Omega_{\text{MF}}/\partial\mu_\downarrow$ . In Fig. 4, we present the momentum distributions of different spin components for the superfluid phase, metastable superfluid phase, and topological superfluid phase, respectively. We found that for both the conventional superfluid phase and the metastable superfluid phase, the momentum distributions of the two spin components exhibit similar trends: higher occupation near zero momentum, decreasing toward the Brillouin zone edge, and displaying 90-degree discrete rotational symmetry due to the cubic lattice, as shown in Fig. 4(a) and (c). In contrast, for the topological superfluid phase in Fig. 4(b), the spin-up particles show a dip-like distribution near zero momentum, while the spin-down distribution remains peaked at the center and decreases toward the edges. This distinctive dip-like feature, unique to the topological superfluid phase, provides a key experimental signature for identi-

fying this state.

#### IV. SUMMARY

In this work, we have systematically studied the many-body phase diagram of a two-component Rashba SOC Fermi gas with two-body loss in a cubic lattice. We show that in the weak interaction regime, the system experiences a sequence of phases—superfluid, normal, and metastable superfluid—as dissipation increases. The intriguing property of many-body phase is the reentrant behavior of superfluid state. In addition, the introduction of Rashba SOC can enlarge the single-particle energy gap, thereby extending the normal phase region and suppressing the superfluid phase in the phase diagram. More importantly, the coexistence of Rashba SOC and a Zeeman field promotes the emergence of topological superfluid states which is robust against local impurities and disturbances as long as the perturbation is not strong enough to close the bulk energy gap and induce a topological phase transition. It would also be interesting to study the possibility of other exotic pairing phases, such as the finite center-of-mass momentum pairing state and the breached paired phase.

#### ACKNOWLEDGMENTS

This work is supported by the National Natural Science Foundation of China (Grant No. 12374046), the Shanghai Science and Technology Innovation Action Plan (Grant No. 24LZ1400800), the State Key Laboratory of Micro-nano Engineering Science (Grant No. MES202605).

---

[1] H. Ramezani, T. Kottos, V. Kovanis, and D. N. Christodoulides, Exceptional-point dynamics in photonic honeycomb lattices with pt symmetry, *Phys. Rev. A* **85**, 013818 (2012).

[2] R. Okugawa and T. Yokoyama, Topological exceptional surfaces in non-hermitian systems with parity-time and parity-particle-hole symmetries, *Phys. Rev. B(R)* **99**, 041202 (2019).

[3] E. J. Bergholtz, J. C. Budich, and F. K. Kunst, Exceptional topology of non-hermitian systems, *Rev. Mod. Phys.* **93**, 015005 (2021).

[4] S. Takemori, K. Yamamoto, and A. Koga, Spin-depairing-induced exceptional fermionic superfluidity, *Phys. Rev. Lett.* **135**, 266002 (2025).

[5] S. Yao and Z. Wang, Edge states and topological invariants of non-hermitian systems, *Phys. Rev. Lett.* **121**, 086803 (2018).

[6] S. Longhi, Probing non-hermitian skin effect and non-bloch phase transitions, *Phys. Rev. Res.* **1**, 023013 (2019).

[7] K. Okuma, Nobuyuki Kawabata, K. Shiozaki, and M. Sato, Topological origin of non-hermitian skin effects, *Phys. Rev. Lett.* **124**, 086801 (2020).

[8] K. Zhang, Z. Yang, and C. Fang, Correspondence between winding numbers and skin modes in non-hermitian systems, *Phys. Rev. Lett.* **125**, 126402 (2020).

[9] L. Zhou, H. Li, W. Yi, and X. Cui, Engineering non-hermitian skin effect with band topology in ultracold gases, *Comm. Phys.* **5**, 252 (2022).

[10] E. Zhao, Z. Wang, C. He, T. F. J. Poon, K. K. Pak, Y.-J. Liu, P. Ren, X.-J. Liu, and G.-B. Jo, Two-dimensional non-hermitian skin effect in an ultracold fermi gas, *Nature* **637**, 565–573 (2025).

[11] Y.-M. Hu, Z. Wang, B. Lian, and Z. Wang, Many-body non-hermitian skin effect with exact steady states in the dissipative quantum link model, *Phys. Rev. Lett.* **135**, 260401 (2025).

[12] C. Chin, R. Grimm, P. Julienne, and E. Tiesinga, Feshbach resonances in ultracold gases, *Rev. Mod. Phys.* **82**, 1225 (2010).

[13] Y.-J. Lin, K. J. García, and I. B. Spielman, Spin-orbit-coupled bose-einstein condensates, *Nature* **471**, 83 (2011).

[14] J.-Y. Zhang, S.-C. Ji, Z. Chen, L. Zhang, Z.-D. Du, B. Yan, G.-S. Pan, B. Zhao, Y.-J. Deng, H. Zhai, S. Chen, and J.-W. Pan, Collective dipole oscillations of a spin-orbit coupled bose-einstein condensate, *Phys. Rev. Lett.* **109**, 115301 (2012).

[15] P. Wang, Z.-Q. Yu, Z. Fu, J. Miao, L. Huang, S. Chai, H. Zhai, and J. Zhang, Spin-orbit coupled degenerate fermi gases, *Phys. Rev. Lett.* **109**, 095301 (2012).

[16] L. W. Cheuk, A. T. Sommer, Z. Hadzibabic, T. Yefsah, W. S. Bakr, and M. W. Zwierlein, Spin-injection spectroscopy of a spin-orbit coupled fermi gas, *Phys. Rev. Lett.* **109**, 095302 (2012).

[17] G. Barontini, R. Labouvie, F. Stubenrauch, A. Vogler, V. Guarnera, and H. Ott, Controlling the dynamics of an open many-body quantum system with localized dissipation, *Phys. Rev. Lett.* **110**, 035302 (2013).

[18] R. Labouvie, B. Santra, S. Heun, and H. Ott, Bistability in a driven-dissipative superfluid, *Phys. Rev. Lett.* **116**, 235302 (2016).

[19] A. Müllers, B. Santra, C. Baals, J. Jiang, J. Benary, R. Labouvie, D. A. Zezyulin, V. V. Konotop, and H. Ott, Coherent perfect absorption of nonlinear matter waves, *Sci. Adv.* **4**, eaat6539 (2018).

[20] J. Li, A. K. Harter, J. Liu, L. de Melo, Y. N. Joglekar, and L. Luo, Observation of parity-time symmetry breaking transitions in a dissipative floquet system of ultracold atoms, *Nat. Comm.* **10**, 855 (2019).

[21] R. Bouganne, M. B. Aguilera, A. Ghermaoui, J. Beugnon, and F. Gerbier, Anomalous decay of coherence in a dissipative many-body system, *Nat. Phys.* **16**, 21 (2020).

[22] Z. J. Ren, D. Liu, E. Zhao, C. He, K. K. Pak, J. S. Li, and G.-B. Jo, Chiral control of quantum states in non-hermitian spin-orbit-coupled fermions, *Nat. Phys.* **18**, 385 (2022).

[23] N. Syassen, D. M. Bauer, M. Lettner, T. Volz, D. Dietze, J. J. Garcia-Ripoll, J. I. Cirac, G. Rempe, and S. Dürr, Strong dissipation inhibits losses and induces correlations in cold molecular gases, *Science* **320**, 1329 (2008).

[24] T. Tomita, S. Nakajima, I. Danshita, Y. Takasu, and Y. Takahashi, Observation of the mott insulator to superfluid crossover of a driven-dissipative bose-hubbard system, *Sci. Adv.* **3**, e1701513 (2017).

[25] K. Sponselee, L. Freystatzky, B. Abeln, M. Diem, B. Hundt, A. Kochanke, T. S. B. Ponath, L. Mathey, K. Sengstock, and Becker.C, Dynamics of ultracold quantum gases in the dissipative fermi-hubbard model, *Quantum Sci. Technol.* **4**, 014002 (2018).

[26] T. Tomita, S. Nakajima, Y. Takasu, and Y. Takahashi, Dissipative bose-hubbard system with intrinsic two-body loss, *Phys. Rev. A* **99**, 031601(R) (2019).

[27] L. Zhou and X. Cui, Effective scattering and efimov physics in the presence of two-body dissipation, *Phys. Rev. Res.* **3**, 043225 (2021).

[28] M. Sun, C. Liu, and Z.-Y. S. Shi, Non-hermitian efimov physics in dissipative three-body systems, *Phys. Rev. Res.* **5**, 043010 (2023).

[29] L. Zhou and X. Cui, Effective scattering and efimov physics in the presence of two-body dissipation, *iScience* **14**, 257 (2019).

[30] L. Zhou, W. Yi, and X. Cui, Dissipation-facilitated molecules in a fermi gas with non-hermitian spin-orbit coupling, *Phys. Rev. A* **102**, 043310 (2020).

[31] X. Zhao and L. Zhou, Stable molecular state under dissipative spin-orbit coupling, *Phys. Rev. A* **108**, 013311 (2023).

[32] K. Yamamoto, M. Nakagawa, K. Adachi, K. Takasan, M. Ueda, and N. Kawakami, Theory of non-hermitian fermionic superfluidity with a complex-valued interaction, *Phys. Rev. Lett.* **123**, 123601 (2019).

[33] M. Iskin, Non-hermitian bcs-bec evolution with a complex scattering length, *Phys. Rev. A* **103**, 013724 (2021).

[34] T. Shi, S. Wang, Z. Zheng, and W. Zhang, Two-dimensional non-hermitian fermionic superfluidity with spin imbalance, *Phys. Rev. A* **109**, 063306 (2024).

[35] A. Ghatak and T. Das, Theory of superconductivity with non-hermitian and parity-time reversal symmetric cooper pairing symmetry, *Phys. Rev. B* **97**, 014512 (2018).

[36] K. Yamamoto, M. Nakagawa, N. Tsuji, M. Ueda, and N. Kawakami, Collective excitations and nonequilibrium phase transition in dissipative fermionic superfluids, *Phys. Rev. Lett.* **127**, 055301 (2021).

[37] H. Tajima, Y. Sekino, D. Inotani, A. Dohi, S. Nagataki, and T. Hayata, Non-hermitian topological fermi superfluid near the *p*-wave unitary limit, *Phys. Rev. A* **107**, 033331 (2023).

[38] M. Nakagawa, N. Kawakami, and U. Masahito, Exact liouvillian spectrum of a one-dimensional dissipative hubbard model, *Phys. Rev. Lett.* **126**, 110404 (2021).

[39] P. C. Burke and A. K. Mitchell, Non-hermitian numerical renormalization group: Solution of the non-hermitian kondo model, *Phys. Rev. Lett.* **135**, 206502 (2025).

[40] X.-J. Liu, Z.-X. Liu, and M. Cheng, Manipulating topological edge spins in a one-dimensional optical lattice, *Phys. Rev. Lett.* **110**, 076401 (2013).

[41] C. Chen, Inhomogeneous topological superfluidity in one-dimensional spin-orbit-coupled fermi gases, *Phys. Rev. Lett.* **111**, 235302 (2013).

[42] W. Zhang and W. Yi, Topological fulde-ferrell-larkin-ovchinnikov states in spin-orbit-coupled fermi gases, *Nat. Comm.* **4**, 2711 (2013).

[43] L.-H. Hu, C.-X. Liu, and F.-C. Zhang, Topological larkin-ovchinnikov phase and majorana zero mode chain in bilayer superconducting topological insulator films, *Nat. Phys.* **2**, 25 (2019).

[44] L. Jiang, X.-J. Liu, H. Hu, and H. Pu, Rashba spin-orbit-coupled atomic fermi gases, *Phys. Rev. A* **84**, 063618 (2011).

[45] C. M. Bender., Making sense of non-hermitian hamiltonians, *Rep. Prog. Phys.* **70**, 947 (2007).

[46] E. G. Moon, P. Nikolić, and S. Sachdev, Superfluid-insulator transitions of the fermi gas with near-unitary interactions in a periodic potential, *Phys. Rev. Lett.* **99**, 230403 (2007).

[47] H. Zhai and T.-L. Ho, Superfluid-insulator transition of strongly interacting fermi gases in optical lattices, *Phys. Rev. Lett.* **99**, 100402 (2007).

[48] Z. Meng, P. Huang, Lianghui and Peng, D. Li, L. Chen, Y. Xu, C. Zhang, P. Wang, and J. Zhang, Experimental observation of a topological band gap opening in ultracold fermi gases with two-dimensional spin-orbit coupling, *Phys. Rev. Lett.* **117**, 235304 (2016).

[49] N. Cooper, J. Dalibard, and I. B. Spielman, Topological bands for ultracold atoms, *Rev. Mod. Phys.* **91**, 015005

(2019).

[50] L.-J. Yang, L.-J. Lang, L. Rong, and H.-P. Hu, Spin-orbit coupled s-wave superconductor in one dimensional optical lattice, *Commun. Theor. Phys.* **63**, 445 (2015).